Collective nonaffine displacements in amorphous materials during large-amplitude oscillatory shear

Nikolai V. Priezjev

Department of Mechanical and Materials Engineering, Wright State University, Dayton, Ohio 45435, USA

Using molecular dynamics simulations, we study the transient response of a binary Lennard-Jones glass subjected to periodic shear deformation. The amorphous solid is modeled as a three-dimensional Kob-Andersen binary mixture at a low temperature. The cyclic loading is applied to slowly annealed, quiescent samples, which induces irreversible particle rearrangements at large strain amplitudes, leading to stress-strain hysteresis and a drift of the potential energy towards higher values. We find that the initial response to cyclic shear near the critical strain amplitude involves disconnected clusters of atoms with large nonaffine displacements. In contrast, the amplitude of shear stress oscillations decreases after a certain number of cycles, which is accompanied by the initiation and subsequent growth of a shear band.

I. INTRODUCTION

The development of advanced thermomechanical processing techniques for metallic glasses might provide access to a broader range of states and thus permit the exploitation of improved material properties [1]. It has been long realized that an elementary plastic event in deformed glasses involves a collective rearrangement of a small group of atoms, known as a shear transformation zone [2–4]. Recently, it was argued that the mechanical yield in amorphous solids does not necessarily result in structural changes but rather represents a transition from a constrained set to a vast number of available configurations [5]. At sufficiently small shear rates, glassy materials exhibit shear localization in the form of fluidized shear bands running across the sample [6,7]. Under a constant strain rate, the plastic flow follows the formation of a percolating cluster of mobile regions characterized by large nonaffine displacements [8,9]. However, shear band initiation and evolution during more complex time-dependent deformation protocols remain relatively unexplored.

In the last several years, the microscopic mechanism of deformation of amorphous materials during periodic shear was studied extensively using atomistic simulations [10–20] and experimental measurements [21–30]. In particular, it was shown that during cyclic loading at small strain amplitudes below the yielding transition, particle trajectories remain reversible over consecutive cycles [11–13,15], and, notably, some atoms undergo repetitive nonaffine displacements with amplitudes that are comparable to the cage size [16,18,29]. It was also found that more slowly cooled glasses undergo smaller particle rearrangements and become more reversible under athermal, quasistatic cyclic shear [20]. In the absence of thermal fluctuations, a sharp onset of particle diffusion is detected at the critical strain amplitude [11–13,15,17], which can be interpreted as a nonequilibrium first-order dynamic phase transition [19]. Rather interestingly, the results of numerical simulations indicate that the yielding transition in oscillatory shear is not accompanied by changes in microscopic structure [19].

At finite temperatures, nonaffine rearrangements in glasses arise both from the thermal motion of atoms and from the imposed shear deformation, and thus shear-induced activation of irreversible structural rearrangements is assisted by thermal

noise [8,18]. Under cyclic loading, atoms with large nonaffine displacements are spatially organized into clusters, which become comparable with the system size near the yield strain [16,18]. Moreover, upon increasing strain amplitude, spatial correlations of nonaffinity become extended over a longer range, although they remain present even in the absence of mechanical deformation due to thermal fluctuations [18]. It was further shown that over many deformation cycles, the structural relaxation dynamics is spatially and temporally heterogeneous; namely, mobile particles, or cage jumps, tend to aggregate into transient clusters [10,14]. Furthermore, during cyclic shear near the yield strain, a cluster of atoms with large reversible nonaffine displacements induces a long-range, time-dependent elastic field that in turn might trigger secondary structural rearrangements. This situation was considered separately in recent studies [31,32], where it was found that a local reversible shear transformation in a quiescent system induces irreversible cage jumps, and their density is larger in the cases of weaker damping or slower shear transformation.

More recently, the fatigue mechanism in bulk metallic glasses subjected to tension-compression cyclic loading was investigated using molecular dynamics (MD) simulations [33] and finite element modeling [34]. It was found that the amplitude of stress oscillations is reduced after the first several cycles, which is associated with the formation of a dominant shear band across the whole system [33,34]. In this process, the initiation of a shear band is preceded by an accumulation of shear transformation zones at the surface of the material. Moreover, it was shown that higher cycling frequency leads to a larger number of cycles to failure [33,34]. Nevertheless, the microscopic details of the relaxation process in amorphous materials under various types of loading conditions remain not fully understood.

In this paper, molecular dynamics simulations are carried out to investigate the transient response of a binary glass to large-amplitude oscillatory shear deformation. It will be shown that above the yield strain, the structural relaxation process involves irreversible rearrangements of particles within a shear band, which leads to stress-strain hysteresis and an increase of the potential energy over consecutive cycles. Near the critical strain amplitude, the formation of a shear band is delayed

for a number of cycles and it coincides with the increase of the potential energy and a distinct drop in the shear stress amplitude.

The rest of the paper is organized as follows. The details of molecular dynamics simulations and the deformation protocol are described in the next section. The variation of the potential energy and shear stress, as well as stress-strain hysteresis and spatial configurations of particles with large nonaffine displacements at different strain amplitudes are presented in Sec. III. The results are briefly summarized in the last section.

II. MOLECULAR DYNAMICS SIMULATIONS

In order to study the deformation dynamics of amorphous materials, we consider the standard Kob-Andersen (KA) (80:20) binary mixture model [35] that was originally designed to reproduce the properties of the metal alloy $Ni_{80}P_{20}$ [36]. In our setup, the system consists of $N_A = 48\,000$ large atoms of type A and $N_B = 12\,000$ small atoms of type B that are confined in a three-dimensional periodic cell. A snapshot of the equilibrated system of $N = 60\,000$ atoms is presented in Fig. 1. In the KA model, any two atoms $\alpha, \beta = A, B$ interact via the truncated Lennard-Jones (LJ) potential as follows,

$$V_{\alpha\beta}(r) = 4\varepsilon_{\alpha\beta}\left[\left(\frac{\sigma_{\alpha\beta}}{r}\right)^{12} - \left(\frac{\sigma_{\alpha\beta}}{r}\right)^{6}\right], \qquad (1)$$

where the interaction parameters are fixed to $\varepsilon_{AA} = 1.0$, $\varepsilon_{AB} = 1.5, \varepsilon_{BB} = 0.5, \sigma_{AB} = 0.8, \sigma_{BB} = 0.88,$ and $m_A = m_B$ [35]. This choice of parameters defines a highly nonadditive LJ potential that prevents crystallization at low temperatures [35]. The cutoff radius is $r_{c,\alpha\beta} = 2.5\sigma_{\alpha\beta}$ and the units of length,
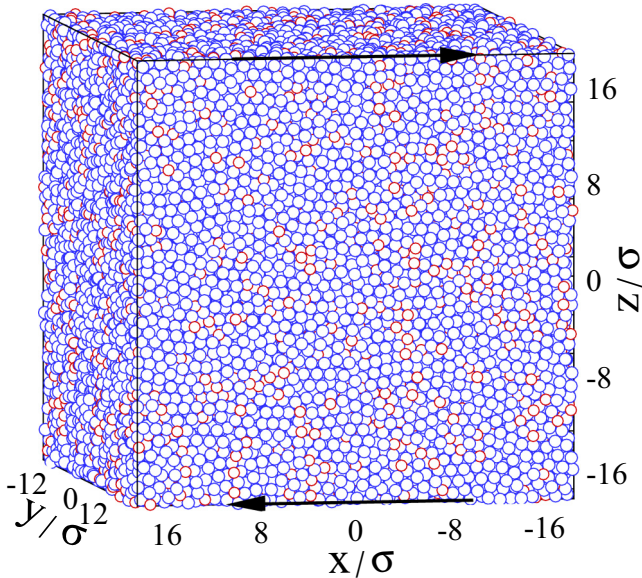

FIG. 1. A snapshot of the instantaneous atomic configuration of the binary Lennard-Jones glass at the temperature $T_{\mathrm{LJ}} = 10^{-2}\varepsilon/k_B$ during periodic shear deformation along the xz plane (indicated by the black arrows) with the strain amplitude $\gamma_0 = 0.10$. The atoms of type A are denoted by large blue circles and atoms of type B are shown by small red circles. Atoms are not drawn to scale. The total number of atoms is $N = 60\,000$.

mass, energy, and time are set to $\sigma = \sigma_{AA}, m = m_A, \varepsilon = \varepsilon_{AA},$ and $\tau = \sigma\sqrt{m/\varepsilon}$, respectively. The equations of motion for each atom were integrated using the Verlet algorithm [37,38] with the time step $\triangle t_{\mathrm{MD}} = 0.005\tau$. The molecular dynamics simulations were conducted using the efficient parallel program LAMMPS developed at Sandia National Laboratories [37].

Each individual sample was carefully prepared by first placing the atoms in the cubic box and assigning random velocities at the temperature $1.1\varepsilon/k_B$, which is above the critical temperature $T_c \approx 0.435\varepsilon/k_B$ [35]. Here, k_B is the Boltzmann constant. The dimensions of the cubic box of linear size $L = 36.84\sigma$ were kept constant in all simulations, and the corresponding density is $\rho = \rho_A + \rho_B = 1.2\sigma^{-3}$. Second, in the absence of mechanical deformation, the temperature of the system was gradually reduced with a computationally slow rate of $10^{-5}\varepsilon/k_B\tau$ to the final temperature $T_{\mathrm{LJ}} = 10^{-2}\varepsilon/k_B$. The data were collected in five independent samples.

Followed by the equilibration procedure, the material was subjected to periodic shear deformation along the xz plane as shown in Fig. 1. The applied shear strain was varied periodically according to

$$\gamma(t) = \gamma_0 \sin(2\pi t/T), \qquad (2)$$

where γ_0 is the strain amplitude and T is the oscillation period. In what follows, the oscillation period was fixed to $T = 5000\tau$ and, correspondingly, the oscillation frequency is $\omega = 2\pi/T = 1.26\times10^{-3}\tau^{-1}$. The Lees-Edwards periodic boundary conditions [38] were employed in the xz plane. The nonequilibrium MD simulations were performed in the constant NVT ensemble, where the temperature was controlled by the dissipative particle dynamics (DPD) thermostat [39]. The DPD thermostat is based on the relative atom velocities and thus the particle dynamics is not coupled to a flow profile, and, as a result, the formation of shear bands or other flow inhomogeneities are not suppressed during deformation of the material [8,39].

III. RESULTS

The initial response of amorphous materials to mechanical deformation depends strongly on the preparation history [1]. In particular, it is well recognized that more slowly annealed glasses acquire a state with a lower potential energy and exhibit higher yield stress [1]. On the other hand, it was shown that large strain cycles cause irreversible relaxations in the material and relocate the system to shallower energy minima, thus leading to rejuvenation [40]. In the present study, the potential energy per particle in one representative sample is plotted in Fig. 2 during 40 cycles for the strain amplitudes $\gamma_0 = 0.07$, 0.08, 0.09, 0.10, 0.12, 0.16, and 0.20. It can be seen that at the strain amplitude $\gamma_0 = 0.07$, the variation of the potential energy is periodic with superimposed noise due to thermal fluctuations. Remarkably, at $\gamma_0 = 0.08$, the potential energy first gradually increases on average during about 20 cycles and then levels off rapidly to a new regime of oscillations with a smaller amplitude. This dynamic transition marks the onset of large-scale irreversible structural rearrangements that will be identified more directly below. As shown in Fig. 2, with further increasing strain amplitude, the potential energy per particle increases more rapidly over consecutive cycles.
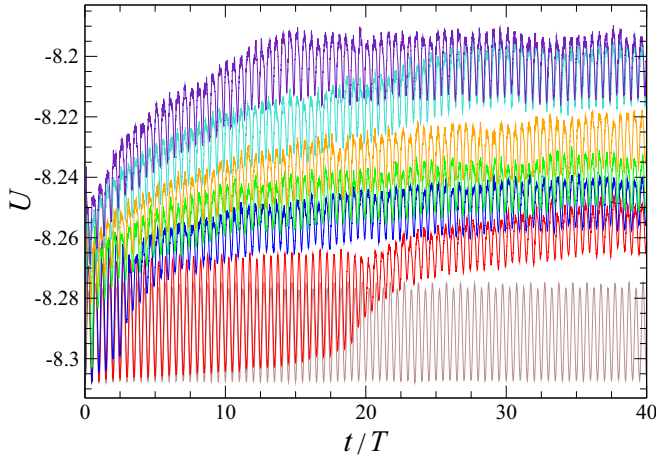
FIG. 2. The variation of the potential energy per particle U (in units of ε) in one sample during the first 40 oscillation cycles for the strain amplitudes $\gamma_0 = 0.07, 0.08, 0.09, 0.10, 0.12, 0.16,$ and 0.20 (from bottom to top). The oscillation period is $T = 5000\tau$.

FIG. 4. The shear stress σ_{xz} (in units of $\varepsilon\sigma^{-3}$) during the first 40 oscillation cycles for the strain amplitudes $\gamma_0 = 0.07$ (brown), 0.08 (red), 0.09 (blue), 0.10 (green), 0.12 (orange), 0.16 (turquoise), and 0.20 (indigo). The period of oscillation is $T = 5000\tau$.

The typical Lissajous curves of shear stress versus strain are displayed in Fig. 3 for the selected strain amplitudes $\gamma_0 = 0.07$, 0.08, 0.10, and 0.20. It can be seen that a small hysteresis, and therefore energy dissipation, appear already at $\gamma_0 = 0.07$, when the system dynamics is nearly reversible, as suggested by the periodic variation of the potential energy shown in Fig. 2. The finite loop area at $\gamma_0 = 0.07$ is masked by the initial response and thermal fluctuations over many cycles. To resolve the hysteresis curve more clearly, the variation of shear stress as a function of strain during the last cycle is also presented in Fig. 3(a). With increasing strain amplitude, the area of the hysteresis loop increases while the amplitude of shear stress remains the same (about $0.72\varepsilon\sigma^{-3}$) in the steady state. Most interestingly, in Fig. 3(b) one can observe a transition from initially small to large hysteresis after several cycles at the strain amplitude $\gamma_0 = 0.08$, which points at enhanced energy dissipation after about 20 cycles. Finally,
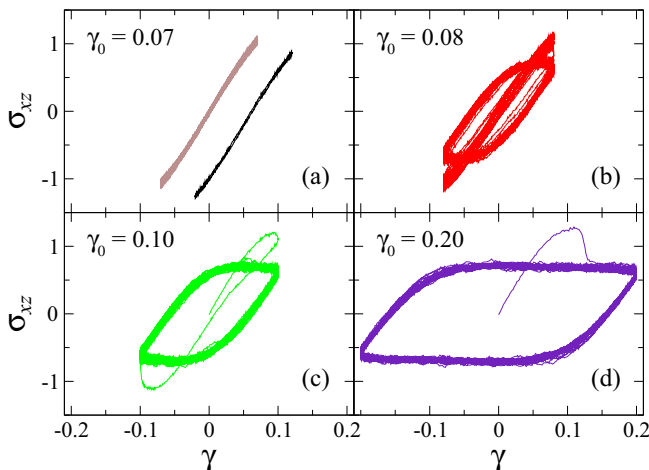
pronounced shear stress overshoots arise during the first cycle, followed by hysteresis loops with large areas at higher strain amplitudes $\gamma_0 = 0.10$ and 0.20, as shown in Figs. 3(c) and 3(d), respectively.

The variation of shear stress during 40 cycles is presented in Fig. 4 for different strain amplitudes. It can be observed that at the strain amplitude $\gamma_0 = 0.07$, the amplitude of shear stress oscillations remains unchanged, which is consistent with the periodic behavior of the potential energy reported in Fig. 2. By contrast, at $\gamma_0 = 0.08$ in Fig. 4, the shear stress amplitude is nearly constant for about 18 cycles and then it decreases to a smaller value, which occurs at the same time when the potential energy grows rapidly (see Fig. 2). This response to applied periodic shear implies a formation of extended fluidized regions that determine the stress amplitude of $0.72 \pm 0.06\varepsilon\sigma^{-3}$. This value correlates well with the postyield shear stress $\sigma_{SS} = 0.68 \pm 0.04\varepsilon\sigma^{-3}$ averaged over five samples under steady shear at the strain rate $\dot{\gamma}\tau = 10^{-4}$ (not shown). Furthermore, it can be seen in Fig. 4 that the shear stress reaches steady-state oscillations after three cycles at $\gamma_0 = 0.09$ and after the first cycle at $\gamma_0 > 0.09$.

It should be noted that the trends identified in Figs. 2–4 were observed in all five independent samples, although the number of cycles until the dynamic transition at the strain amplitude $\gamma_0 = 0.08$ varies from 15 to 59. These results agree qualitatively with recent numerical simulations of metallic glasses under tension-compression cyclic loading, where it was shown that after a certain number of cycles, the stress amplitude is reduced concomitantly with the initiation of a shear band across the sample [33,34]. We also comment that the transition from reversible dynamics at $\gamma_0 = 0.07$ to the plastic regime at $\gamma_0 = 0.08$ occurs at higher strain amplitudes than the critical value $\gamma_0 = 0.06$ reported in the previous MD study [10], where simulations were performed at the higher oscillation frequency $\omega\tau = 0.02$ and higher temperature $T_{LJ} = 0.1\varepsilon/k_B$. At the same time, our results are in agreement with the critical strain amplitude $\gamma_0 = 0.07$, which marks the onset of energy dissipation and particle diffusion in a binary

FIG. 3. The shear stress σ_{xz} (in units of $\varepsilon\sigma^{-3}$) vs shear strain γ during 40 cycles for the strain amplitudes (a) $\gamma_0 = 0.07$, (b) $\gamma_0 = 0.08$, (c) $\gamma_0 = 0.10$, and (d) $\gamma_0 = 0.20$. The data for the last cycle at $\gamma_0 = 0.07$ are included in (a) and displaced for clarity (black curve).
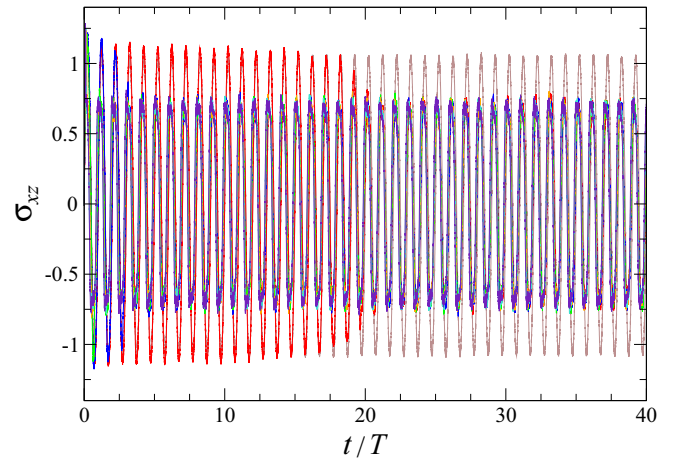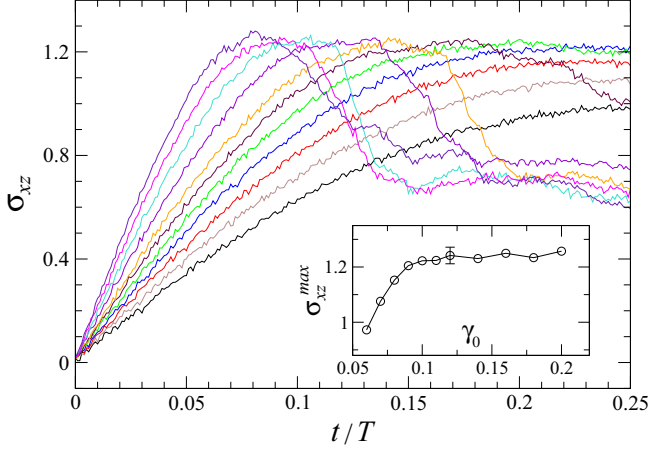
FIG. 5. The shear stress σ_{xz} (in units of $\varepsilon\sigma^{-3}$) during the first cycle for the strain amplitudes $\gamma_0 = 0.06, 0.07, 0.08, 0.09, 0.10, 0.11, 0.12, 0.14, 0.16, 0.18,$ and 0.20 (from right to left). The period of oscillation is $T = 5000\tau$. The data are taken in one sample. The inset shows the value of the overshoot stress averaged over five samples as a function of the strain amplitude.
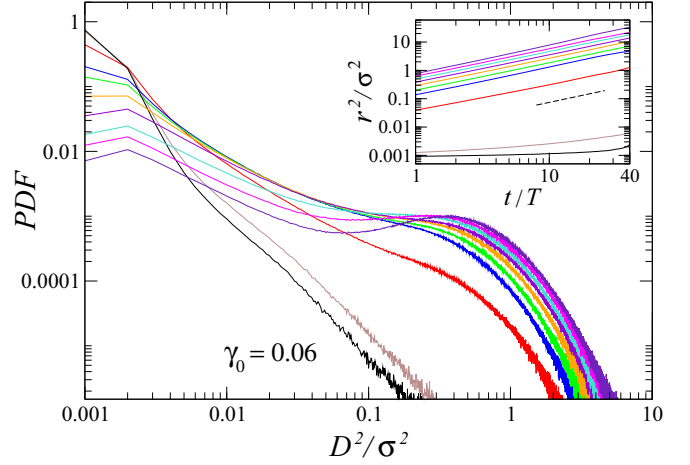

FIG. 6. The normalized probability distribution function of $D^2(t,T)$ after one cycle for the strain amplitudes $\gamma_0 = 0.06, 0.07, 0.08, 0.09, 0.10, 0.12, 0.14, 0.16, 0.18,$ and 0.20 (from left to right). The inset shows the mean square displacement of atoms for the same strain amplitudes (from bottom to top). The straight dashed line with unit slope is plotted for reference.

glass under oscillatory athermal quasistatic shear deformation [11,17].

To show the initial response more clearly, the time dependence of the shear stress during the first quarter of the cycle is presented in Fig. 5 for different strain amplitudes. It can be seen that the yield stress becomes apparent at $\gamma_0 \geqslant 0.08$. As expected, the overshoot stress increases with increasing strain amplitude or average strain rate. Typical strain rates at $t = 0$ are $\dot{\gamma}\tau = 7.54 \times 10^{-5}$ for $\gamma_0 = 0.06$ and $\dot{\gamma}\tau = 2.51 \times 10^{-4}$ for $\gamma_0 = 0.20$. The inset in Fig. 5 shows the averaged value of the overshoot stress as a function of the strain amplitude.

We next perform a more detailed microscopic analysis that involves spatial configurations of atoms with large relative displacements during periodic shear. In general, a combination of a linear transformation and a translation defines the so-called affine deformation of the material. In turn, a deviation from the linear strain field can be described by a nonaffine component of displacement of atoms relative to their neighbors. The nonaffine measure is defined via the transformation matrix $\mathbf{J}_i$ [4] that best maps all bonds between the ith atom and neighboring atoms during the time interval Δt as follows,

$$D^2(t, \Delta t) = \frac{1}{N_i} \sum_{j=1}^{N_i} \{\mathbf{r}_j(t + \Delta t) - \mathbf{r}_i(t + \Delta t)$$
$$- \mathbf{J}_i[\mathbf{r}_j(t) - \mathbf{r}_i(t)]\}^2, \qquad (3)$$

where the sum is taken over N_i nearest-neighbor atoms within the distance 1.5σ from $\mathbf{r}_i(t)$. In what follows, the quantity $D^2(t, \Delta t)$ was evaluated during $\Delta t = T$ with respect to atomic configurations at zero strain. Note that in the definition of the nonaffine measure, Eq. (3), D^2 is normalized by the number of neighbors in the first shell, and therefore the value $D^2 \approx 0.01\sigma^2$ corresponds approximately to a displacement of the atom $\mathbf{r}_i$ on the order of the cage size with respect to its neighbors.

The probability distribution function of the nonaffine measure is plotted in Fig. 6 for the selected strain amplitudes. The quantity $D^2(t,T)$ was computed after each cycle with respect to zero strain, i.e., at $t = 0, T, \ldots, 39T$. The data in Fig. 6 were averaged over five independent samples and 40 oscillation cycles. It is evident that at the strain amplitudes $\gamma_0 = 0.06$ and 0.07, the distribution function decays rapidly at small values of D^2, which implies that most of the atoms return to their cages after each cycle. We comment that some atoms with $D^2 > 0.01\sigma^2$ after one cycle might return back to their cages after several cycles, which does not necessarily lead to structural relaxation of the material. Examples of reversible cage jumps during 50 oscillation cycles were reported in the previous MD study [16]. With increasing strain amplitude, $\gamma_0 \geqslant 0.08$, the shape of the probability distribution function becomes more broad, and it acquires a local maximum at $D^2 > 0.1\sigma^2$ and $\gamma_0 \geqslant 0.18$. The appearance of large nonaffine displacements at $\gamma_0 \geqslant 0.08$ indicates a large number of cage breaking events and it suggests that at least a part of the material becomes fluidized. These conclusions are consistent with the abrupt change of the mean square displacement from a subdiffusive plateau at small strain amplitudes $\gamma_0 \leqslant 0.07$ to a diffusive behavior at $\gamma_0 \geqslant 0.08$, which is shown in the inset of Fig. 6.

Further insight into the structural relaxation process can be gained by examining the spatial configurations of atoms with large nonaffine displacements. Examples of particle positions with $D^2(t,T) > 0.01\sigma^2$ are presented in Figs. 7–10 for different strain amplitudes. In each case, the quantity $D^2(t,T)$ was evaluated for each atom after a full back-and-forth cycle with respect to the selected reference times that correspond to zero strain. It can be observed in Fig. 7 that during cyclic loading at the strain amplitude $\gamma_0 = 0.07$, atoms with large nonaffine displacements tend to aggregate into disconnected clusters. Interestingly, the number of atoms with $D^2(0,T) > 0.01\sigma^2$ is larger after the first cycle, indicating significant rearrangements of atoms with respect to their equilibrium
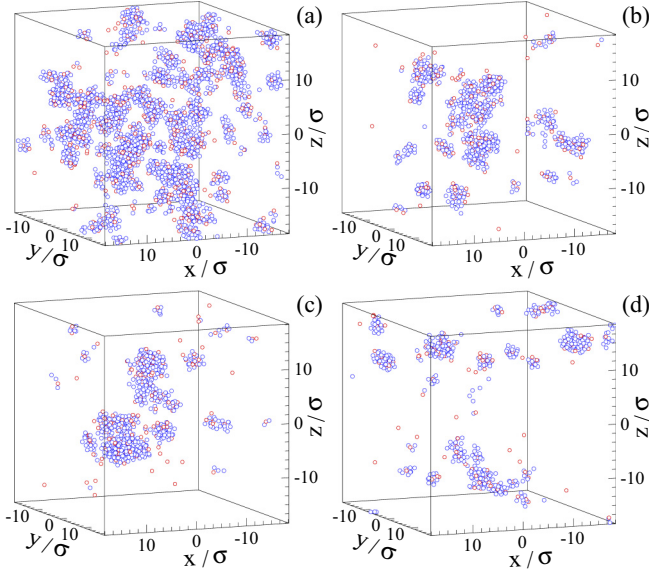
FIG. 7. Instantaneous atomic configurations for the strain amplitude $\gamma_0 = 0.07$ and the nonaffine measure (a) $D^2(0,T) > 0.01\sigma^2$, (b) $D^2(9T,T) > 0.01\sigma^2$, (c) $D^2(19T,T) > 0.01\sigma^2$, and (d) $D^2(39T,T) > 0.01\sigma^2$. The atoms of types A and B are marked by blue and red circles, respectively.

positions in the annealed sample, which is followed by a steady process with smaller scattered clusters. A similar trend with the initial decrease of the number of rearrangements with large irreversible displacements was observed in periodically sheared suspensions below the strain threshold [21].

The most striking observation from the sequence of snapshots shown in Fig. 8 for the strain amplitude $\gamma_0 = 0.08$ is the transition from initial nonpercolating clusters of atoms with
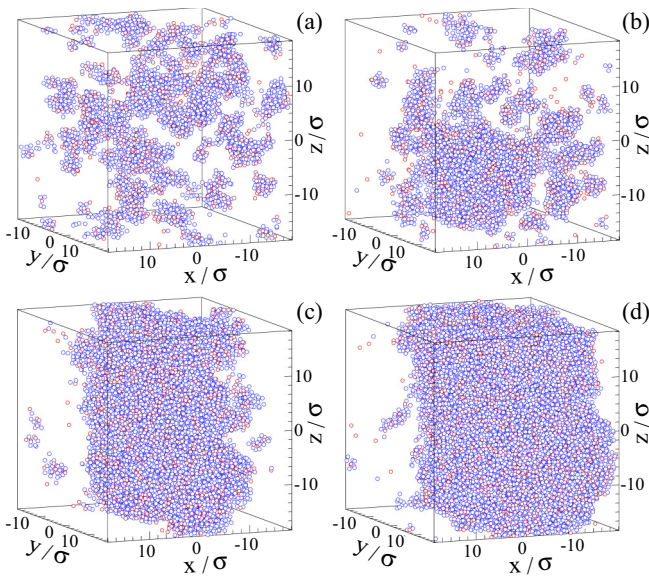

FIG. 8. Snapshots of atom positions for the strain amplitude $\gamma_0 = 0.08$ and the nonaffine measure (a) $D^2(0,T) > 0.01\sigma^2$, (b) $D^2(9T,T) > 0.01\sigma^2$, (c) $D^2(19T,T) > 0.01\sigma^2$, and (d) $D^2(39T,T) > 0.01\sigma^2$.
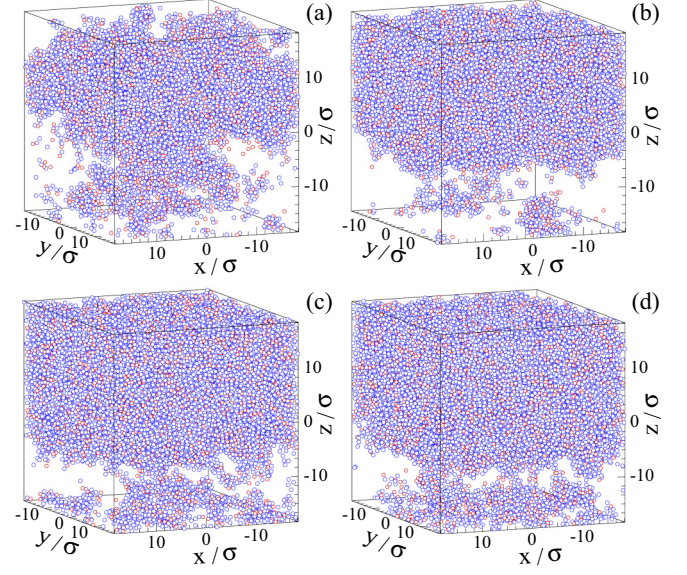

FIG. 9. Configurations of atoms of types A and B for the strain amplitude $\gamma_0 = 0.10$ and the nonaffine measure (a) $D^2(0,T) > 0.01\sigma^2$, (b) $D^2(9T,T) > 0.01\sigma^2$, (c) $D^2(19T,T) > 0.01\sigma^2$, and (d) $D^2(39T,T) > 0.01\sigma^2$.

$D^2 > 0.01\sigma^2$ to the formation of the shear band across the whole system after the 20th cycle. Note that this dynamic transition correlates well with the drop in amplitude of the shear stress oscillations for $\gamma_0 = 0.08$ shown in Fig. 4 and with the increase in the potential energy in Fig. 2. Thus, once the system-spanning shear band is formed, the maximum shear stress during periodic loading is determined by the fluidized region. We observed that the orientation of a shear band is parallel to either yz or xy planes in different samples. This is consistent with the formation of shear bands parallel or perpendicular to the shear flow direction in binary LJ glasses subjected to a constant strain rate [8]. It also should be mentioned that a discontinuous transition from a reversible dynamics to a diffusive behavior upon increasing strain amplitude resembles a first-order phase transition; however, the appearance of a percolating cluster of mobile atoms in a form of a shear band is a signature of a continuous transition.

As is evident from Fig. 9, the shear band is formed parallel to the xy plane during the first oscillation cycle at the strain amplitude $\gamma_0 = 0.10$. Over the next 40 cycles, the width of the shear band gradually increases, however, it remains smaller than the system size. Note that a single shear band is extended in the $\hat{z}$ direction via periodic boundary conditions in Figs. 9(c) and 9(d). Furthermore, as shown in Fig. 10, the shear band appears at the first cycle for the strain amplitude $\gamma_0 = 0.16$, and the whole sample becomes fluidized after the 30th cycle [see Fig. 10(d)]. With further increasing strain amplitude, the number of cycles required for atoms with large nonaffine displacements to be distributed uniformly throughout the system decreases (not shown).

Taken together, the results in this study for the potential energy, stress-strain hysteresis, shear stress, and spatial distribution of nonaffine displacements indicate that the yielding transition occurs at strain amplitudes $0.07 < \gamma_0 < 0.08$. This
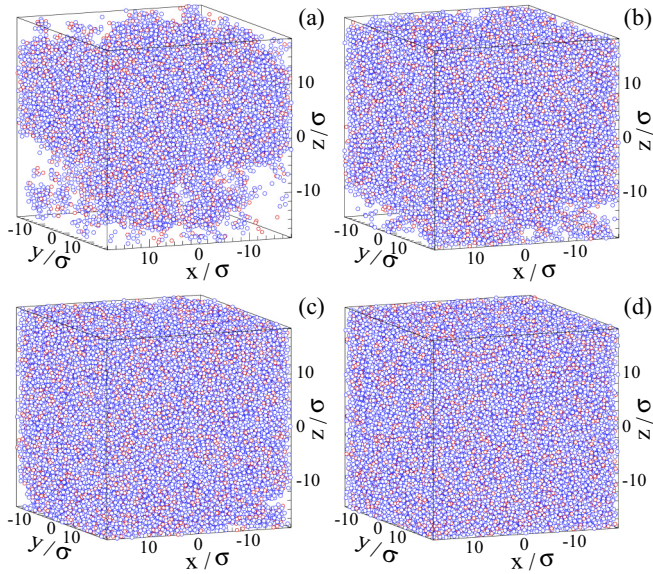
FIG. 10. Positions of atoms A and B for the strain amplitude $\gamma_0 = 0.16$ and the nonaffine measure (a) $D^2(0,T) > 0.01\sigma^2$, (b) $D^2(9T,T) > 0.01\sigma^2$, (c) $D^2(19T,T) > 0.01\sigma^2$, and (d) $D^2(29T,T) > 0.01\sigma^2$.

is consistent with the crossover from exponential to power-law decay (when the strain amplitude is varied from $\gamma_0 = 0.07$ to 0.08) of the spatial correlation function of nonaffine displacements reported in the previous study [18]. At larger strain amplitudes, the cyclic deformation induces irreversible nonaffine rearrangements of atoms within a shear band that reduce the amplitude of shear stress oscillations. We finally comment that in accordance with the nucleation picture of the yielding transition, where the formation of a shear band delays the onset of plastic flow, the critical strain amplitude at very low shear rates can be significantly lower than the value $\gamma_0 = 0.08$.

IV. CONCLUSIONS

In summary, the dynamic response of binary LJ glasses to oscillatory shear was investigated using molecular dynamics simulations. The periodic shear strain was applied to quiescent samples that were prepared by cooling down with a computationally slow rate to a temperature well below the glass transition. It should be emphasized that temperature was regulated by the dissipative particle dynamics thermostat that avoids profile biasing and thus represents a good choice for studying problems that involve flow localization.

It was found that during cyclic loading near the critical strain amplitude, the relaxation process involves transient, nonpercolating clusters of atoms with large nonaffine displacements for a number of cycles, which are followed by the formation of a shear band running across the sample. The appearance of the shear band causes a noticeable drop in the shear stress amplitude and marks the onset of irreversible particle rearrangements leading to a sharp increase of the potential energy. With increasing strain amplitude, the stress-strain hysteresis becomes more pronounced and the plastic flow develops in the whole sample.

In the future, it will be interesting to determine more precisely the critical strain amplitude that sets irreversible nonaffine displacements and to explore its dependence on temperature, oscillation frequency, system size, and preparation history.

[1] Y. Sun, A. Concustell, and A. L. Greer, Thermomechanical processing of metallic glasses: Extending the range of the glassy state, Nat. Rev. Mater. **1**, 16039 (2016).

[2] F. Spaepen, A microscopic mechanism for steady state inhomogeneous flow in metallic glasses, Acta Metall. **25**, 407 (1977).

[3] A. S. Argon, Plastic deformation in metallic glasses, Acta Metall. **27**, 47 (1979).

[4] M. L. Falk and J. S. Langer, Dynamics of viscoplastic deformation in amorphous solids, Phys. Rev. E **57**, 7192 (1998).

[5] P. K. Jaiswal, I. Procaccia, C. Rainone, and M. Singh, Mechanical Yield in Amorphous Solids: A First-Order Phase Transition, Phys. Rev. Lett. **116**, 085501 (2016).

[6] F. Varnik, L. Bocquet, J.-L. Barrat, and L. Berthier, Shear Localization in a Model Glass, Phys. Rev. Lett. **90**, 095702 (2003).

[7] Y. Shi and M. L. Falk, Atomic-scale simulations of strain localization in three-dimensional model amorphous solids, Phys. Rev. B **73**, 214201 (2006).

[8] G. P. Shrivastav, P. Chaudhuri, and J. Horbach, Yielding of glass under shear: A directed percolation transition precedes shear-band formation, Phys. Rev. E **94**, 042605 (2016).

[9] G. P. Shrivastav, P. Chaudhuri, and J. Horbach, Heterogeneous dynamics during yielding of glasses: Effect of aging, J. Rheol. **60**, 835 (2016).

[10] N. V. Priezjev, Heterogeneous relaxation dynamics in amorphous materials under cyclic loading, Phys. Rev. E **87**, 052302 (2013).

[11] D. Fiocco, G. Foffi, and S. Sastry, Oscillatory athermal quasistatic deformation of a model glass, Phys. Rev. E **88**, 020301(R) (2013).

[12] I. Regev, T. Lookman, and C. Reichhardt, Onset of irreversibility and chaos in amorphous solids under periodic shear, Phys. Rev. E **88**, 062401 (2013).

[13] C. F. Schreck, R. S. Hoy, M. D. Shattuck, and C. S. O'Hern, Particle-scale reversibility in athermal particulate media below jamming, Phys. Rev. E **88**, 052205 (2013).

[14] N. V. Priezjev, Dynamical heterogeneity in periodically deformed polymer glasses, Phys. Rev. E **89**, 012601 (2014).

[15] I. Regev, J. Weber, C. Reichhardt, K. A. Dahmen, and T. Lookman, Reversibility and criticality in amorphous solids, Nat. Commun. **6**, 8805 (2015).

[16] N. V. Priezjev, Reversible plastic events during oscillatory deformation of amorphous solids, Phys. Rev. E **93**, 013001 (2016).

[17] P. Leishangthem, A. D. S. Parmar, and S. Sastry, The yielding transition in amorphous solids under oscillatory shear deformation, arXiv:1612.02629.

[18] N. V. Priezjev, Nonaffine rearrangements of atoms in deformed and quiescent binary glasses, Phys. Rev. E **94**, 023004 (2016).

[19] T. Kawasaki and L. Berthier, Macroscopic yielding in jammed solids is accompanied by a nonequilibrium first-order transition in particle trajectories, Phys. Rev. E **94**, 022615 (2016).

[20] M. Fan, M. Wang, K. Zhang, Y. Liu, J. Schroers, M. D. Shattuck, and C. S. O'Hern, The effects of cooling rate on particle rearrangement statistics: Rapidly cooled glasses are more ductile and less reversible, arXiv:1607.04221.

[21] L. Corte, P. M. Chaikin, J. P. Gollub, and D. J. Pine, Random organization in periodically driven systems, Nat. Phys. **4**, 420 (2008).

[22] R. Candelier, O. Dauchot, and G. Biroli, Building Blocks of Dynamical Heterogeneities in Dense Granular Media, Phys. Rev. Lett. **102**, 088001 (2009).

[23] N. Koumakis, J. F. Brady, and G. Petekidis, Complex Oscillatory Yielding of Model Hard-Sphere Glasses, Phys. Rev. Lett. **110**, 178301 (2013).

[24] N. C. Keim and P. E. Arratia, Yielding and microstructure in a 2D jammed material under shear deformation, Soft Matter **9**, 6222 (2013).

[25] E. D. Knowlton, D. J. Pine, and L. Cipelletti, A microscopic view of the yielding transition in concentrated emulsions, Soft Matter **10**, 6931 (2014).

[26] R. Jeanneret and D. Bartolo, Geometrically protected reversibility in hydrodynamic Loschmidt-echo experiments, Nat. Commun. **5**, 3474 (2014).

[27] M. C. Rogers, K. Chen, L. Andrzejewski, S. Narayanan, S. Ramakrishnan, R. L. Leheny, and J. L. Harden, Echoes in x-ray speckles track nanometer-scale plastic events in colloidal gels under shear, Phys. Rev. E **90**, 062310 (2014).

[28] K. H. Nagamanasa, S. Gokhale, A. K. Sood, and R. Ganapathy, Experimental signatures of a nonequilibrium phase transition governing the yielding of a soft glass, Phys. Rev. E **89**, 062308 (2014).

[29] M. T. Dang, D. Denisov, B. Struth, A. Zaccone, and P. Schall, Reversibility and hysteresis of the sharp yielding transition of a colloidal glass under oscillatory shear, Eur. Phys. J. E **39**, 44 (2016).

[30] T. Gibaud, C. Perge, S. B. Lindstrom, N. Taberlet, and S. Manneville, Multiple yielding processes in a colloidal gel under large amplitude oscillatory stress, Soft Matter **12**, 1701 (2016).

[31] N. V. Priezjev, Plastic deformation of a model glass induced by a local shear transformation, Phys. Rev. E **91**, 032412 (2015).

[32] N. V. Priezjev, The effect of a reversible shear transformation on plastic deformation of an amorphous solid, J. Phys.: Condens. Matter **27**, 435002 (2015).

[33] Z. D. Sha, S. X. Qu, Z. S. Liu, T. J. Wang, and H. Gao, Cyclic deformation in metallic glasses, Nano Lett. **15**, 7010 (2015).

[34] Y. Jiang, Numerical modeling of cyclic deformation in bulk metallic glasses, Metals **6**, 217 (2016).

[35] W. Kob and H. C. Andersen, Testing mode-coupling theory for a supercooled binary Lennard-Jones mixture: The van Hove correlation function, Phys. Rev. E **51**, 4626 (1995).

[36] T. A. Weber and F. H. Stillinger, Local order and structural transitions in amorphous metal-metalloid alloys, Phys. Rev. B **31**, 1954 (1985).

[37] S. J. Plimpton, Fast parallel algorithms for short-range molecular dynamics, J. Comput. Phys. **117**, 1 (1995); see also http://lammps.sandia.gov/

[38] M. P. Allen and D. J. Tildesley, *Computer Simulation of Liquids* (Clarendon Press, Oxford, UK, 1987).

[39] T. Soddemann, B. Dunweg, and K. Kremer, Dissipative particle dynamics: A useful thermostat for equilibrium and nonequilibrium molecular dynamics simulations, Phys. Rev. E **68**, 046702 (2003).

[40] D. J. Lacks and M. J. Osborne, Energy Landscape Picture of Overaging and Rejuvenation in a Sheared Glass, Phys. Rev. Lett. **93**, 255501 (2004).